PROCEEDINGS OF SCIENCE

The Optical and Mechanical Design of POEMMA Balloon with Radio

Eric Mayotte,[a,*] Austin Cummings,[b] Paul Degarate,[c] Neville DeWitt Pierrat,[d] Johannes Eser,[e] William Finch,[f] Julia Burton-Heibges,[a] Tobias Heibges,[a] Eric Mentzell,[g] Stephan Meyer,[h] Conrad Shay,[a] Benjamin Stillwell,[h] Yoshiyuki Takizawa,[i] Luke Wanner[a] and Lawrence Wiencke[a] for the JEM-EUSO Collaboration

[a] *Department of Physics, Colorado School of Mines, 1523 Illinois St., Golden, CO, USA*
[b] *Department of Physics, Pennsylvania State University, 251 Pollock Rd, University Park, PA, USA*
[c] *Halley Tech Inc, 2257 Arlington Ct, Auburn Al, USA*
[d] *Firebrand Engineering,* `contact@firebrand.engineering`*, Golden CO, USA*
[e] *Columbia Astrophysics Laboratory, Columbia University, 538 West 120th Street, New York, NY, USA*
[f] *Cotopaxi Mech,* `https://cotopaximech.com`*, Denver CO, USA*
[g] *NASA Goddard Space Flight Center, 8800 Greenbelt Rd, Greenbelt, MD, USA*
[h] *Department of Astronomy & Astrophysics, University of Chicago, 5640 S Ellis Ave, Chicago, IL, USA*
[i] *Center for Advanced Photonics, RIKEN, 2-1 Hirosawa, Wako, Saitama, Japan*

E-mail: `emayotte@mines.edu`

POEMMA Balloon with Radio (PBR) is a NASA super-pressure balloon mission building toward the proposed Probe Of Extreme Multi-Messenger Astrophysics (POEMMA) dual satellite mission. In its planned 2027 launch, PBR will study Ultra-High-Energy Cosmic Rays, Neutrinos, and High-Altitude Horizontal Airshowers from 33 km above the Earth. By operating at balloon altitudes, PBR will provide a novel vantage point to study air-shower physics while offering competitive instantaneous exposure to neutrinos from transient astrophysical phenomena. The payload's optical instrument is a 0.95 m^2 aperture hybrid Schmidt telescope with a 3.81 m^2 segmented mirror focusing light onto a Fluorescence Camera and a bi-focalized Cherenkov Camera. The payload will also feature a Radio Instrument consisting of two sinuous antennas based on the Payload for Ultrahigh Energy Observations (PUEO) low-frequency instrument. A combined gamma ray/x-ray detector and IR cloud camera round out the instrumentation package, meaning PBR will be the first multi-hybrid balloon-borne multi-messenger observatory flown. This extensive instrumentation must be combined into a radio quiet payload that satisfies the scientific needs and can operate in near vacuum at extreme temperatures, all while meeting NASA safety requirements and weighing no more than 3000 lbs (1361 kg). Accomplishing these tasks together will mark a significant step toward establishing technological readiness for the POEMMA satellite mission. We present an overview of PBR's mechanical and optical systems, additionally detailing our strategies to mitigate electromagnetic interference for the radio instrument and prepare for the harsh near-space environment.

39th International Cosmic Ray Conference (ICRC2025)
15–24 July 2025
Geneva, Switzerland

*Speaker

PoS(ICRC2025)332

1. POEMMA Balloon with Radio

The study of ultra-high-energy cosmic rays (UHECRs) and Very-High-Energy Neutrinos (VHE-ν) has progressed significantly over the last twenty years, driven by the high precision and large exposures of modern ground-based observatories. However, fundamental questions about their origins and nature remain unanswered, particularly at the highest energies. Resolving these will likely require next-generation observatories offering substantially improved resolution and/or orders-of-magnitude larger exposure [1]. Space-based instruments present a practical route to such exposure, surveying vast atmospheric volumes from a single platform. The proposed dual-satellite Probe of Multi-Messenger Astrophysics (POEMMA) mission aims to extend the exposure limits for both UHECRs and VHE-νs simultaneously by exploiting this approach [2].

In the development of space-based observatories, pathfinder balloon missions are crucial for validating detection techniques and advancing technological readiness prior to full-scale satellite deployments. POEMMA Balloon with Radio (PBR) is the third and most advanced Super Pressure Balloon (SPB) pathfinder mission undertaken by the JEM-EUSO collaboration and is planned to fly from New Zealand in early 2027 (for a detailed overview, see [3]). Leveraging the successes and experience from previous balloon missions, EUSO-SPB1 [4] and EUSO-SPB2 [5], PBR significantly upgrades observational capabilities compared to earlier balloon payloads. PBR incorporates a hybrid focal surface combining a Fluorescence Camera (FC) [6] and Cherenkov Camera (CC) [7] into a Schmidt telescope, following the design proposed for POEMMA. PBR also uniquely adds simultaneous radio, X-ray, and γ-ray detection capabilities allowing for multi-channel multi-hybrid observations of air showers [8]. Furthermore, the PBR telescope can rotate freely in azimuth and point from nadir to +15° above the horizon to target different phenomena and follow up on astrophysical alerts. This combination of instrumentation makes PBR the first multi-hybrid high-energy stratospheric astroparticle observatory, enabling it to pursue its primary science goals:

1. **Investigating the Origin of UHECRs:** PBR will perform the first sub-orbital measurement of extensive air shower (EAS) fluorescence induced by UHECRs, validating key detection technologies planned for POEMMA.
2. **Studying High-Altitude Horizontal Air-Showers (HAHAs):** PBR's unique stratospheric vantage point will enable the first extensive study of rarely observed HAHAs. Simultaneous detection through optical Cherenkov, radio, X-ray, and γ-ray instruments will provide a multi-hybrid characterization of highly extended air showers developing in rarefied atmospheres, facilitating precise measurements of cosmic-ray spectrum near PeV energies.
3. **Searching for Astrophysical Neutrinos:** PBR will provide high instantaneous exposure to Earth-skimming tau neutrinos via below-horizon EAS detections using Cherenkov and radio instruments. This capability enables fast follow-ups of transient multi-messenger sources.

2. The General Design of the PBR Payload

The PBR payload comprises the mechanical structure and scientific instrumentation package carried aboard the NASA SPB. It hosts all instruments essential to achieving PBR's scientific goals, while conforming to rigorous NASA flight and safety requirements. Each component must withstand conditions such as pressures down to 1 mbar, temperatures as low as −70° C, and accelerations exceeding 8 G with considerable margins of safety. Although the standard maximum payload

weight for NASA balloons is 2500 lbs (1134 kg), PBR has been granted an exception, increasing its allowable science payload to 3000 lbs (1361 kg). Additionally, minimizing electromagnetic interference is critical for the successful operation of the sensitive radio instrument. Meeting these constraints simultaneously presents significant engineering challenges.

Fig. 1 provides a schematic overview of the payload's layout and main components. The **Rotator** connects the superpressure balloon to the payload gondola, allowing precise azimuthal rotation control to 1° accuracy [9], with absolute pointing determined with sub-1° accuracy via differential GPS. The **Gondola** provides the structural framework and mounting points for all payload subsystems. It is made out of aerospace-grade (7075) Aluminum alloy angle with steel nut blocks and rigging points for a high-strength, low-weight combination assembly. The **Power System** includes a *Battery Box*, housing seven high-capacity batteries, heaters, and power-management electronics; a *Primary Solar Array*, consisting of 27 lightweight, high-efficiency panels that actively track the sun via the Rotator; and a *Backup Solar Array* of five fixed panels to ensure safe operation in case of Rotator failure.

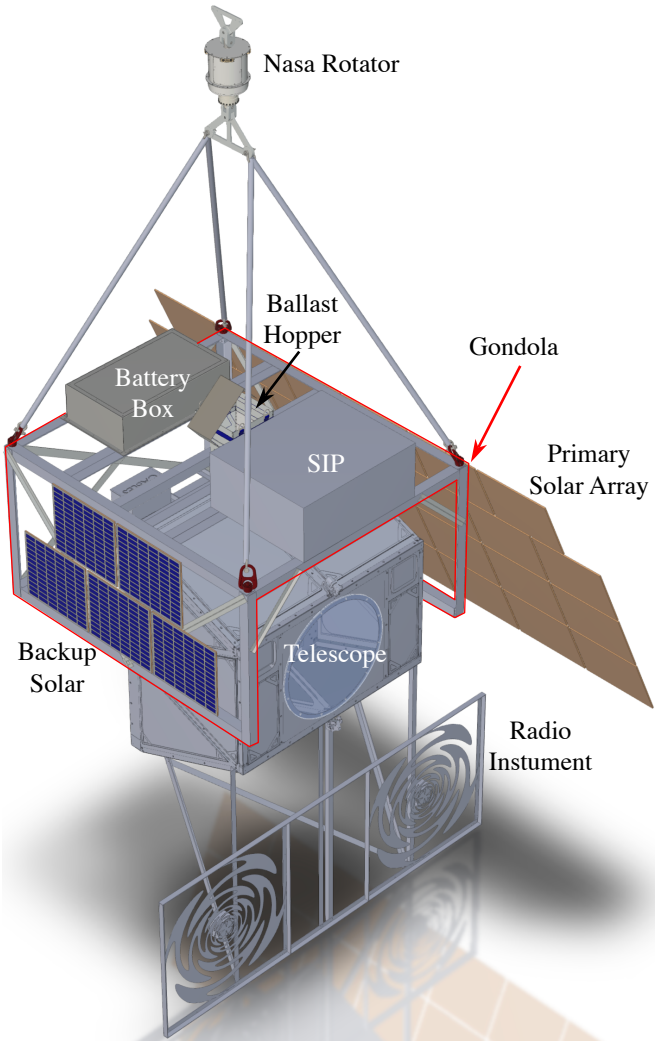

Figure 1: Overview of the PBR Payload

The **Ballast Hopper**, a NASA standard system, stores and dispenses up to 600 lbs (272 kg) of ballast to regulate balloon altitude. NASA also provides the **Support Instrumentation Package (SIP)**, which handles telemetry, communication, and command functions. The **Telescope** is the primary scientific instrument (see Sec. 4), housing the optical system (Sec. 3), CC[7], FC[6], X-ray/γ-ray detector [8], the IR cloud camera, calibration equipment, and the control computers for the these instruments and as well as the radio [10].

The **Radio Instrument** includes two antennas modeled after the Payload for Ultrahigh Energy Observations (PUEO)'s low-frequency antenna [11], along with their support structures and deployment mast (see Sec. 5). This instrument operates in conjunction with the Cherenkov detector, measuring radio emissions from EASs in the frequency range from approximately 50 to 500 MHz. Lastly, the **Vertical Rotator** adjusts the elevation pointing of the Telescope and Radio Instrument from nadir to +15° above the horizon, achieving steering accuracy around 0.1°, with precise pointing direction verified by onboard inclinometers [12].

3. PBR Optics

The PBR telescope is of Schmidt design for several reasons. Schmidt telescopes offer a fast focal ratio, allowing the telescope to accommodate a large aperture within a compact and lightweight assembly. They provide a wide, well-corrected Field-of-View (FoV) with few optical parts, maximizing sensitivity and ensuring uniform image quality across PBR's large hybrid focal surface. Schmidt telescopes also allow for the use of a spherically curved mirror, significantly simplifying the mirror design and fabrication costs, while also simplifying the mechanical design of the mirror support frame. Additionally, only a thin Aspheric Corrector Plate (ACP) is required, which keeps the payload mass and volume low. Last, their straightforward and squat design allows the sturdy construction needed to minimize flexing without adding unmanageable weight to the payload. An optical diagram of the PBR Schmidt telescope is shown in Fig. 2.

The PBR telescope needs to support a $27° \times 36°$ FoV and a 1.1 m diameter, 0.95 m^2 aperture. As shown in Fig. 3, to achieve this, it features an approximately 1.82 m × 2 m, 3.81 m^2 segmented spherical mirror with a ~ 1.66 m Radius of Curvature (RoC) and a large ACP to minimize distortion at the edges of the FoV. As shown in Fig. 3, the mirror is composed of 12 trapezoidal segments with a slightly different geometry for the middle rows as compared to the top and bottom rows. All segments are made of 11 mm-thick, vacuum-slumped, borosilicate glass with a vacuum-deposited aluminum film layer optimized for reflectivity in the UV, which is protected by a silicon dioxide coating. Both mirror segments weigh ~ 18 lbs (8.16 kg). The other main optical component is the polymethyl methacrylate (PMMA) ACP, which sits at the aperture to correct distortions at the edge of FoV. It has been shaped in a precision diamond-turning process to a thickness of 10 mm in the center, which tapers to ~ 5 mm at its lowest point near the edges, after which it is polished.

To fit the CC and FC, the $27° \times 36°$ FoV focal surface is approximately 38 cm × 51.4 cm in size and has an RoC of ~ 853 mm. The four Photo Detection Modules (PDMs) of the FC occupy the top focal surface with a $27° \times 27°$ FoV. Because the detection surface of each FC PDM is flat, a field flattener is placed in front of each to map the spherical focal surface to the PDM face. To limit background contamination, each PDM also has a BG3 filter placed over the detection surface,

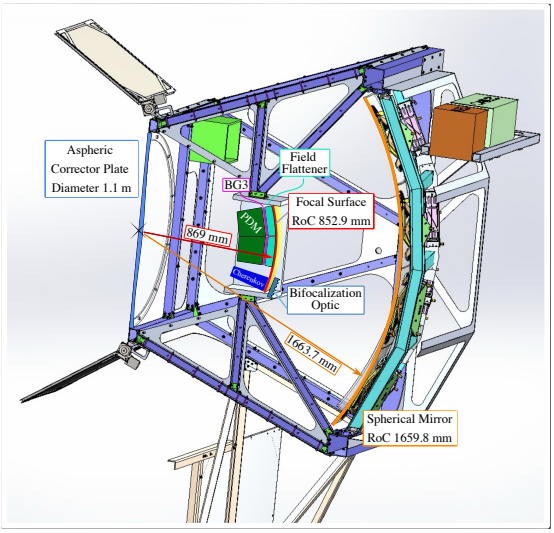

Figure 2: The Optical Sketch of PBR

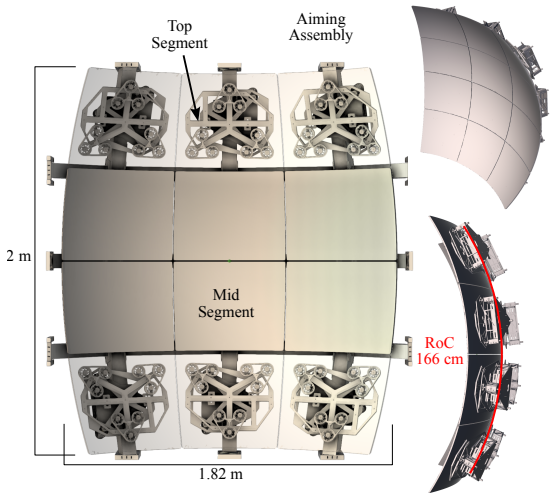

Figure 3: The Primary Mirror of PBR

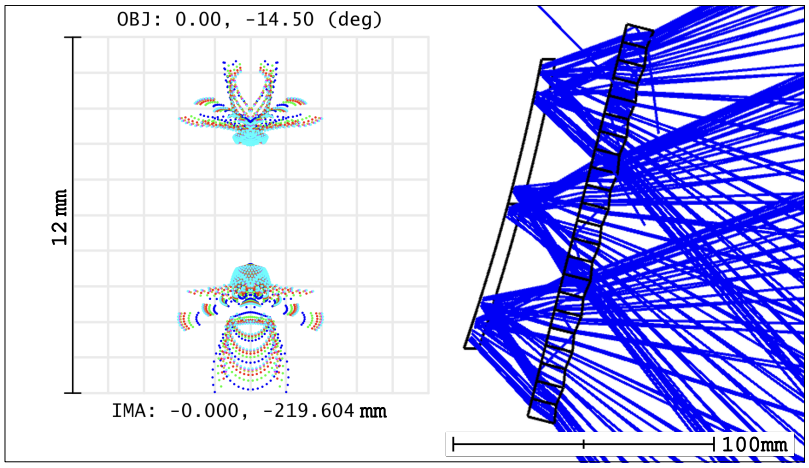

Figure 4: The Cherenkov Camera Bifocalization Optics. Right: Zemax simulation of a prototype diagram of a vertical biafocalization optic placed in front of the focal surface of the CC. Left: spot diagram from a bifocalizer built to produce a ~ 6 mm spot separation (2 pixels) showing the majority of light is well contained within a single 3×3 mm pixel.

allowing only wavelengths between 290 nm and 430 nm to reach the camera.

The CC sits at the bottom of the focal surface, occupying $12° \times 6°$ of the FoV. The CC features a curved detection face which closely follows the focal surface RoC. As shown in Fig. 4, in the current design, bifocalization optics (Bifocalizer) are positioned in front of the CC to split the optical signal into two well-separated pixels. The performance of the Bifocalizer is being evaluated. In case the performance is insufficient for reliable low-threshold triggering in the CC, aiming the mirror segments to create the two desired spots on the CC is also being explored. The optical signal of the CC is split into two non-adjacent pixels to provide a clear veto of direct charge particle strikes to the camera, as only light that reaches the telescope nearly parallel will be split, indicating that the event occurred far from the telescope. The remaining angular space of the focal surface is taken up by the mechanical requirements of holding and supporting the cameras and optics.

4. PBR Telescope Mechanics

The mechanical structure of the telescope was designed to support the optical prescription described above. Like any steerable telescope, the structure had to be rigid enough to prevent the sagging of any optical components due to gravity when moving over its full range of pointing. In contrast to any telescope placed on the ground, except for in the most extreme circumstances, the telescope of PBR must also preserve optical performance and structural integrity over a temperature range of $-70°$ C to $25°$ C and accelerations has high as 8 G with considerable safety factors. Furthermore, it must survive in near-vacuum and high-UV environments without the ability to repair any components that fail during flight. The structure designed to meet these challenges is shown in Fig. 5, with the rear mirror support cage (shown in Fig. 3) removed for visibility.

The ruling mechanical constraint is the optical stiffness of the assembly, as this is a higher bar than the yield constraints imposed by NASA. Since 6061 and 7075 Aluminum alloys have very similar Young's moduli, and 6061 is cheaper, easier to procure, and is available in more form factors, 6061 has been chosen as the alloy used for the majority of the telescope. The exception applies to the flexure assemblies described below and a select few other components, where yield was observed within the safety margins on the upper end of the possible acceleration range. The telescope structure can be broken down into five major components: the mirror assembly, the telescope frame, the aperture assembly, the camera shelf, and the dark-box shell.

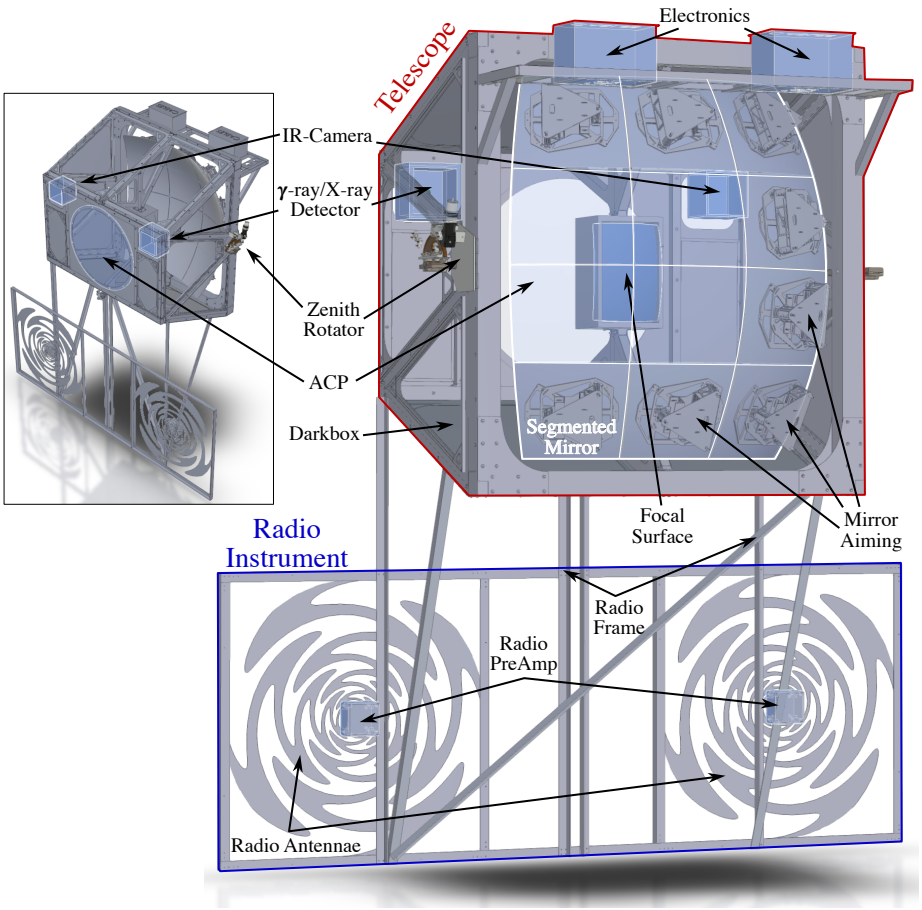

Figure 5: The Telescope Assembly of PBR

Telescope Frame The core of the telescope frame is the large square belt frame, which wraps vertically around the mirror, just behind the center of mass of the telescope. The belt frame bears the majority of the telescope's load, stiffens it, and directly interfaces with the rotator system. The Mirror Assembly bolts directly to this belt, providing very high stiffness to minimize sag in any aiming direction. From this belt, two trusses extend forward on both sides of the belt frame to hold the aperture assembly in place. In the center of the telescope, an additional smaller truss extends forward to the aperture assembly to hold the camera shelf in place. On the outside of these trusses, gussets are built in to stiffen the assembly and hold the panels of the dark box shell. Due to weight concerns, the material of the telescope frame has been minimized in all recognized opportunities.

Aperture Assembly The Aperture Assembly must do three main things: it must hold the ACP firmly in place, it must hold and orient the IR-Camera and γ/X-ray detector (indicated in Fig. 5), and it must hold the shutters (seen in Fig. 2). To maintain the required stiffness, the front of the aperture assembly is skinned with an Aluminum sheet with peepholes for the IR-Camera and γ/X-ray detector. The shutters are mounted to the top/bottom of the assembly on the central trusses.

Dark-Box shell The Dark box panels are composed of a layered structure. Reflective Mylar forms the outermost layer, reflecting solar radiation and keeping the telescope temperatures low during the day. Under the Mylar sits a layer of Titan RF Faraday fabric [13] to transform the telescope

into a Faraday cage, thereby suppressing EMI from the various electronics within the telescope. Next is a 19 mm thick layer of high-density extruded polyurethane foam to insulate the telescope from extreme cold and heat at float. Finally, a layer of light-absorbing paint or foil is applied to suppress stray light within the telescope, to lower measurement backgrounds. This structure has been incorporated into paneling, which covers the Telescope Frame and Mirror Assembly.

Mirror Assembly The mirror assembly, shown in Fig. 3, consists of 12 mirror cells and the mirror support cage. A conceptual sketch of a mirror cell is shown in Fig. 6. Working left to right, first, there is the mirror segment. Next are nine pads made of Kovar, which are glued to the mirror segment using Scotch weld D2216 Epoxy and 3901 primer. Kovar alloy and the specific epoxy have the same or similar thermal properties as the glass in the mirrors, meaning the bond to the glass remains strong over the full range of temperatures faced by the payload. To attach the pads to the rest of the Aluminum assembly, flexures are used, which have been designed to absorb the force due to the thermal contraction difference between aluminum and the glass of the mirrors. The flexures are placed into a Whipple tree assembly to distribute loads equally among the nine pads. Targeted testing of the pad/glass bond shows it reliably holds more than 400 lbs (181.4 kg) at −60° C, well below the lowest temperature expected for the mirror. In FEA, the maximum per pad load seen under a 100° C ΔT and an 8 G shock is 45.7 lbs (20.7 kg). Next, there is the aiming plate, which allows for the mirrors to be steered to achieve the desired focus on the cameras. Lastly, there are the frame mounting plates that secure the mirror cell to the mirror support frame.

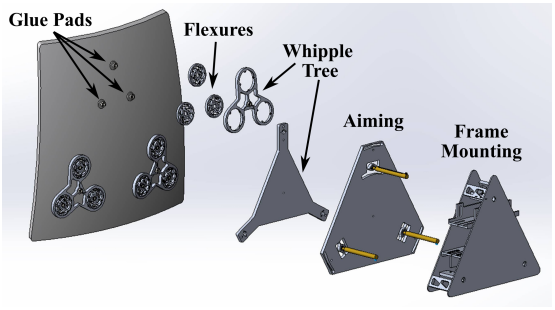

Figure 6: Mirror Cell

Camera Shelf The last mechanical component of the PBR Telescope is the camera shelf. The camera shelf serves as the interface point between the telescope frame and the FC and CC. It will allow the two cameras to be independently moved ±2.5 cm along the optical access while minimizing obscuration of the cameras or mirror. Its design is still being finalized as the geometries and support structures of the FC and CC are still being designed.

5. PBR Radio Instrument Mechanics

The radio instrument and assembly can be seen extending from the bottom of the telescope in Fig. 5. The main mechanical requirements on the radio assembly are: that it must fix the orientation of the radio antenna so that their normal vectors are parallel to the optical axis of the telescope within 1°, that the assembly survives an 8 G shock with a safety factor of 1.5, that the radio is free from obscuration of any metal components within its 60° × 60° FoV, that the total assembly weighs no more than 150 lbs (68kg), and that the whole assembly is free from conductive components save for nuts, bolts and dedicated radio electronics.

The most challenging aspect of meeting all these requirements was identifying procurable non-conductive materials that could withstand these loads at −70° C within the budget. Ultimately, a combination of materials was necessary. The mast assembly, which extends from the telescope

to the radio antenna, is to be constructed from Glass Fiber Reinforced Vinylester (GFRV), which has excellent strength properties and is readily available in the required lengths and geometries. At joints, due to concerns with possible tear out, Glass-reinforced epoxy laminate #10 (G10) gussets and bolt plates are employed. The Radio Antennas are printed in copper on Flame Retardant 4 glass-reinforced epoxy laminate (FR4) sheets, which have been sandwiched onto an Aramid honeycomb to provide stiffness. This combination yields very light, yet stiff, antenna assemblies with exceptional gain. The frame that supports the antenna is a composite structure, consisting of FR4 blocking incorporated into the antenna panels themselves, paired with GFRV bars to provide the required inter-antenna separation. The amplification electronics are bolted directly onto the back of the antenna panels. The full assembly is bolted directly to the telescope frame, providing a stiff and lightweight assembly that meets all requirements.

6. Outlook

The development and construction of PBR is on track for an early 2027 flight. The mechanical design of the PBR payload is nearing completion, and the project is now moving to the fabrication and construction phase. The majority of components will be ready by the end of 2025 and will then be sent to the Colorado School of Mines in Golden, Colorado, for integration during the Spring of 2026. After integration, the telescope will be field-tested in Utah at the Telescope Array site [14] to profile the performance of the instrumentation in the Summer of 2026. After field tests, in the Fall of 2026, PBR will be sent to the Columbia Scientific Balloon Facility (CSBF) facility in Palestine, Texas, for hang testing and final flight approval. From CSBF, PBR will be shipped to Wanaka, New Zealand, for flight on a super-pressure balloon in early 2027. When flown, PBR will make novel astroparticle observations from the stratosphere and will represent a significant step towards the proposed next-generation space-based UHECR / VHE-ν Observatory POEMMA [2].

References

[1] A. Coleman et al., *Astropart. Phys.* **149** (2023) 102819 [2205.05845].
[2] A.V. Olinto et al., [POEMMA Coll.], *JCAP* **06** (2021) 007 [2012.07945].
[3] J. Eser et al., [JEM-EUSO Coll.], *PoS(ICRC2025)249* (2025) These proceedings.
[4] G. Abdellaoui et al., [JEM-EUSO Coll.], *Astropart. Phys.* **154** (2024) 102891 [2401.06525].
[5] J.H. Adams, Jr. et al., 2505.20762.
[6] F. Cafagna et al., [JEM-EUSO Coll.], *PoS(ICRC2025)209* (2025) These proceedings.
[7] V. Scotti et al., [JEM-EUSO Coll.], *PoS(ICRC2025)391* (2025) These proceedings.
[8] M. Battisti et al., [JEM-EUSO Coll.], *PoS(ICRC2025)* (2025) These proceedings.
[9] C.E. Burth, COSPAR (2022), Available via NASA NTRS.
[10] V. Scotti et al., [JEM-EUSO Coll.], *PoS(ICRC2025)392* (2025) These proceedings.
[11] Q. Abarr et al., *Journal of Instrumentation* **16** (2021) P08035.
[12] L. Wiencke et al., [JEM-EUSO Coll.], *PoS(ICRC2025)* (2025) These proceedings.
[13] MOS Equipment https://mosequipment.com/products/titanrf-faraday-fabric, 2020.
[14] M. Fukushima, *Prog. Theor. Phys. Suppl.* **151** (2003) 206.

Acknowledgments

The authors would like to acknowledge the support by NASA award 80NSSC22K1488 and 80NSSC24K1780, by the French space agency CNES and the Italian Space agency ASI. The work is supported by OP JAC financed by ESIF and the MEYS CZ.02.01.01/00/22_008/0004596. We gratefully acknowledge the collaboration and expert advice provided by the PUEO collaboration. We also acknowledge the invaluable contributions of the administrative and technical staffs at our home institutions.

Full Authors list: The JEM-EUSO Collaboration

M. Abdullahi[ep,er] M. Abrate[ek,el], J.H. Adams Jr.[ld], D. Allard[cb], P. Alldredge[ld], R. Aloisio[ep,er], R. Ammendola[ei], A. Anastasio[ef], L. Anchordoqui[le], V. Andreoli[ek,el], A. Anzalone[eh], E. Arnone[ek,el], D. Badoni[ei,ej], P. von Ballmoos[ce], B. Baret[cb], D. Barghini[ek,em], M. Battisti[ei], R. Bellotti[ea,eb], A.A. Belov[ia,ib], M. Bertaina[ek,el], M. Betts[lm], P. Biermann[da], F. Bisconti[ee], S. Blin-Bondil[cb], M. Boezio[ey,ez] A.N. Bowaire[ek,el] I. Buckland[ez], L. Burmistrov[ka], J. Burton-Heibges[lc], F. Cafagna[ea], D. Campana[ef,eu], F. Capel[db], J. Caraca[lc], R. Caruso[ec,ed], M. Casolino[ei,ej], C. Cassardo[ek,el], A. Castellina[ek,em], K. Černý[ba], L. Conti[en], A.G. Coretti[ek,el], R. Cremonini[ek,ev], A. Creusot[cb], A. Cummings[lm], S. Davarpanah[ka], C. De Santis[ei], C. de la Taille[ca], A. Di Giovanni[ep,er], A. Di Salvo[ek,el], T. Ebisuzaki[fc], J. Eser[ln], F. Fenu[eo], S. Ferrarese[ek,el], G. Filippatos[lb], W.W. Finch[lc], C. Fornaro[en], C. Fuglesang[ja], P. Galvez Molina[lp], S. Garbolino[ek], D. Garg[li], D. Gardiol[ek,em], G.K. Garipov[ia], A. Golzio[ek,ev], C. Guépin[cd], A. Haungs[da], T. Heibges[lc], F. Isgrò[ef,eg], R. Iuppa[ew,ex], E.G. Judd[la], F. Kajino[fb], L. Kupari[li], S.-W. Kim[ga], P.A. Klimov[ia,ib], I. Kreykenbohm[dc] J.F. Krizmanic[lj], J. Lesrel[cb], F. Liberatori[ej], H.P. Lima[ep,er], E. M'sihid[cb], D. Mandát[bb], M. Manfrin[ek,el], A. Marcelli[ei], L. Marcelli[ei], W. Marszał[ha], G. Masciantonio[ei], V.Masone[ef], J.N. Matthews[lg], E. Mayotte[lc], A. Meli[lo], M. Mese[ef,eg,eu], S.S. Meyer[lb], M. Mignone[ek], M. Miller[li], H. Miyamoto[ek,el], T. Montaruli[ka], J. Moses[lc], R. Munini[ey,ez] C. Nathan[lj], A. Neronov[cb], R. Nicolaidis[ew,ex], T. Nonaka[fa], M. Mongelli[ea], A. Novikov[lp], F. Nozzoli[ex], T. Ogawa[fc], S. Ogio[fa], H. Ohmori[fc], A.V. Olinto[ln], Y. Onel[li], G. Osteria[ef,eu], B. Panico[ef,eg,eu], E. Parizot[cb,cc], G. Passeggio[ef], T. Paul[ln], M. Pech[ba], K. Penalo Castillo[le], F. Perfetto[ef,eu], L. Perrone[es,et], C. Petta[ec,ed], P. Picozza[ei,ej,fc], L.W. Piotrowski[hb], Z. Plebaniak[ei], G. Prévôt[cb], M. Przybylak[hd], H. Qureshi[ef,eu], E. Reali[ei], M.H. Reno[li], F. Reynaud[ek,el], E. Ricci[ew,ex], M. Ricci[ei,ee], A. Rivetti[ek], G. Saccà[ed], H. Sagawa[fa], O. Saprykin[ic], F. Sarazin[lc], R.E. Saraev[ia,ib], P. Schovánek[bb], V. Scotti[ef,eg,eu], S.A. Sharakin[ia], V. Scherini[es,et], H. Schieler[da], K. Shinozaki[ha], F. Schröder[lp], A. Sotgiu[ei], R. Sparvoli[ei,ej], B. Stillwell[lb], J. Szabelski[hc], M. Takeda[fa], Y. Takizawa[fc], S.B. Thomas[lg], R.A. Torres Saavedra[ep,er], R. Triggiani[ea], C. Trimarelli[ep,er], D.A. Trofimov[ia], M. Unger[da], T.M. Venters[lj], M. Venugopal[da], C. Vigorito[ek,el], M. Vrabel[ha], S. Wada[fc], D. Washington[lm], A. Weindl[da], L. Wiencke[lc], J. Wilms[dc], S. Wissel[lm], I.V. Yashin[ia], M.Yu. Zotov[ia], P. Zuccon[ew,ex].

[ba] Palacký University, Faculty of Science, Joint Laboratory of Optics, Olomouc, Czech Republic
[bb] Czech Academy of Sciences, Institute of Physics, Prague, Czech Republic
[ca] École Polytechnique, OMEGA (CNRS/IN2P3), Palaiseau, France
[cb] Université de Paris, AstroParticule et Cosmologie (CNRS), Paris, France
[cc] Institut Universitaire de France (IUF), Paris, France
[cd] Université de Montpellier, Laboratoire Univers et Particules de Montpellier (CNRS/IN2P3), Montpellier, France
[ce] Université de Toulouse, IRAP (CNRS), Toulouse, France
[da] Karlsruhe Institute of Technology (KIT), Karlsruhe, Germany
[db] Max Planck Institute for Physics, Munich, Germany
[dc] University of Erlangen–Nuremberg, Erlangen, Germany
[ea] Istituto Nazionale di Fisica Nucleare (INFN), Sezione di Bari, Bari, Italy
[eb] Università degli Studi di Bari Aldo Moro, Bari, Italy
[ec] Università di Catania, Dipartimento di Fisica e Astronomia "Ettore Majorana", Catania, Italy
[ed] Istituto Nazionale di Fisica Nucleare (INFN), Sezione di Catania, Catania, Italy
[ee] Istituto Nazionale di Fisica Nucleare (INFN), Laboratori Nazionali di Frascati, Frascati, Italy
[ef] Istituto Nazionale di Fisica Nucleare (INFN), Sezione di Napoli, Naples, Italy
[eg] Università di Napoli Federico II, Dipartimento di Fisica "Ettore Pancini", Naples, Italy
[eh] INAF, Istituto di Astrofisica Spaziale e Fisica Cosmica, Palermo, Italy
[ei] Istituto Nazionale di Fisica Nucleare (INFN), Sezione di Roma Tor Vergata, Rome, Italy
[ej] Università di Roma Tor Vergata, Dipartimento di Fisica, Rome, Italy
[ek] Istituto Nazionale di Fisica Nucleare (INFN), Sezione di Torino, Turin, Italy
[el] Università di Torino, Dipartimento di Fisica, Turin, Italy
[em] INAF, Osservatorio Astrofisico di Torino, Turin, Italy
[en] Università Telematica Internazionale UNINETTUNO, Rome, Italy
[eo] Agenzia Spaziale Italiana (ASI), Rome, Italy

PoS(ICRC2025)332

[ep] Gran Sasso Science Institute (GSSI), L'Aquila, Italy
[er] Istituto Nazionale di Fisica Nucleare (INFN), Laboratori Nazionali del Gran Sasso, Assergi, Italy
[es] University of Salento, Lecce, Italy
[et] Istituto Nazionale di Fisica Nucleare (INFN), Sezione di Lecce, Lecce, Italy
[eu] Centro Universitario di Monte Sant'Angelo, Naples, Italy
[ev] ARPA Piemonte, Turin, Italy
[ew] University of Trento, Trento, Italy
[ex] INFN–TIFPA, Trento, Italy
[ey] IFPU – Institute for Fundamental Physics of the Universe, Trieste, Italy
[ez] Istituto Nazionale di Fisica Nucleare (INFN), Sezione di Trieste, Trieste, Italy
[fa] University of Tokyo, Institute for Cosmic Ray Research (ICRR), Kashiwa, Japan
[fb] Konan University, Kobe, Japan
[fc] RIKEN, Wako, Japan
[ga] Korea Astronomy and Space Science Institute, South Korea
[ha] National Centre for Nuclear Research (NCBJ), Otwock, Poland
[hb] University of Warsaw, Faculty of Physics, Warsaw, Poland
[hc] Stefan Batory Academy of Applied Sciences, Skierniewice, Poland
[hd] University of Lodz, Doctoral School of Exact and Natural Sciences, Łódź, Poland
[ia] Lomonosov Moscow State University, Skobeltsyn Institute of Nuclear Physics, Moscow, Russia
[ib] Lomonosov Moscow State University, Faculty of Physics, Moscow, Russia
[ic] Space Regatta Consortium, Korolev, Russia
[ja] KTH Royal Institute of Technology, Stockholm, Sweden
[ka] Université de Genève, Département de Physique Nucléaire et Corpusculaire, Geneva, Switzerland
[la] University of California, Space Science Laboratory, Berkeley, CA, USA
[lb] University of Chicago, Chicago, IL, USA
[lc] Colorado School of Mines, Golden, CO, USA
[ld] University of Alabama in Huntsville, Huntsville, AL, USA
[le] City University of New York (CUNY), Lehman College, Bronx, NY, USA
[lg] University of Utah, Salt Lake City, UT, USA
[li] University of Iowa, Iowa City, IA, USA
[lj] NASA Goddard Space Flight Center, Greenbelt, MD, USA
[lm] Pennsylvania State University, State College, PA, USA
[ln] Columbia University, Columbia Astrophysics Laboratory, New York, NY, USA
[lo] North Carolina A&T State University, Department of Physics, Greensboro, NC, USA
[lp] University of Delaware, Bartol Research Institute, Department of Physics and Astronomy, Newark, DE, USA

PoS(ICRC2025)332